NASA TECHNICAL MEMORANDUM

NASA TM X-71489

NASA TM X-71489

THE DRIFT FIELD MODEL APPLIED TO THE LITHIUM-CONTAINING SILICON SOLAR CELL

by Michael P. Godlewski, Cosmo R. Baraona,
and Henry W. Brandhorst, Jr.
Lewis Research Center
Cleveland, Ohio 44135

TECHNICAL PAPER proposed for presentation at
Tenth Photovoltaic Specialists Conference sponsored by
the Institute of Electrical and Electronics Engineers
Palo Alto, California, November 13-15, 1973

THE DRIFT FIELD MODEL APPLIED TO THE LITHIUM-CONTAINING SILICON SOLAR CELL

Michael P. Godlewski, Cosmo R. Baraona
and Henry W. Brandhorst, Jr.

National Aeronautics and Space Administration
Lewis Research Center
Cleveland, Ohio

E-7025

SUMMARY

The drift field model used by Wolf to calculate the short-circuit current (I_{sc}) was extended to permit calculations of the open-circuit voltage (V_{oc}) and the maximum power (P_m) under conditions of illumination of either tungsten (2800° C) source or AMO sunlight. Voltages were calculated using an expression for the drift field diode saturation current derived here. The model, applied to the oxygen rich (C-13 group) lithium solar cells, was used to calculate the pre- and post-electron bombardment trends of the V_{oc}, P_m, and I_{sc} for lithium gradients in the range of 10^{18} to 10^{19} Li/cm^4. Published experimental data characterizing these cells were used to tailor the model. The calculated trends are in reasonable agreement with the empirical data of Faith. Diffusion length degradation and carrier removal effects were sufficient to predict the cell performance up to 3×10^{14} e/cm^2. Beyond this fluence it was necessary to include drift field removal effects.

INTRODUCTION

The unusual performance of lithium-containing solar cells has been studied by several investigators (1-3). In order to explain the self-healing effects of these cells when exposed to a radiation environment, it has been proposed that the lithium neutralizes the radiation induced defects resulting in less severe effect on cell performance. Recently Faith (4, 5) has measured, using a tungsten light source, the open circuit voltage (V_{oc}), short circuit current (I_{sc}), and maximum power (P_m) of oxygen rich (C-13 group) lithium cells exposed to 1 MeV electrons in the 3×10^{13} to 3×10^{15} e/cm^2 fluence range. From these data, empirical formulae were constructed which relate the radiation behavior to the magnitude of the lithium gradient near the junction. Additional work by Iles (6) had shown that unbombarded cell performance can be correlated with the lithium gradient. In addition Faith et al. (7) have considered a case in which the lithium gradient gives rise to an internal electric field.

Although a drift field model has been developed and applied to calculate the short circuit current performance (8-10), the model has not been used to analyze the open circuit voltage or the maximum power of the lithium cell. Thus it is the purpose of this paper to formulate a general field model for the lithium solar cell, to use this model to calculate the current, voltage, and power of the cell, and to predict the initial and radiation bombarded performance. The model will be applied specifically to the C-13 group of lithium cells, since the electrical performance of these cells is well documented. The formulation for I_{sc} obtained by Wolf (8) and the diode saturation current derived here will be used to obtain the V_{oc} from the simple diode equation. The maximum power and cell curve factor are also calculated. These equations include drift field effects and apply to the low injection case.

REVIEW OF PREVIOUS EXPERIMENTAL WORK

Lithium Gradient and Cell Performance

The calculations using the four layer drift field model are based on measurements of the lithium profile and diffusion length for the C-13 group of oxygen-rich, lithium-diffused p on n solar cells published by Faith (4, 5) and Iles (6). These data are summarized in Table I for nominal lithium concentrations evaluated at the junction edge (x_j), at the rear contact (W), and at the subregion edge (X). The preirradiated cell performance, e.g., V_{oc}, P_m, I_{sc}, and lithium profile, was measured for cells in this group and was found to correlate with the lithium gradient at the junction edge. The high voltage cells, which had a high gradient (~ 10^{19} cm^{-4}), were fabricated in short lithium diffusion times (375° C - 180 min). Using experimental data, it was estimated that the gradient extended over a region 3 μm thick next to the junction. Similarly, cells which were diffused for longer times (325° C - 480 min) had a lower gradient (~ 10^{18} cm^{-4}) and also a lower V_{oc} compared to the high gradient cells. The subregion thickness for this case was estimated to be about 10 to 20 μm. Cells diffused in the short times had higher measured lithium concentrations everywhere in the n-base, than were cells diffused for longer times. No experimental diffusion schedule can be assigned to the medium gradient (5×10^{18}) cells. However, it is thought that these gradients are a result of the 375° - 180 min diffusion and extend over a thickness that is intermediate to the high and low gradient cases. Correlations of the lithium gradient with the measured values of I_{sc} and P_m were also made. In these cases however the trend appears to be that the highest values of I_{sc} and P_m occur for the low gradient and the lowest values for the high gradient. The carrier lifetimes shown in Table I represent nominal data representative of each type cell.

Empirical Bombardment Data

Measurements of the V_{oc}, P_m, and I_{sc} of selected C-13 cells after exposure to 1 MeV electron fluences in the range of 3×10^{13} to 3×10^{15} e/cm^2 have been reported by Faith (4, 5). A tungsten light source was used for cell evaluation. From these data empirical formulae were developed that reflect a dependence of each cell parameter on the electron fluence and on the lithium gradient (dN/dx). These relationships which are valid only in the above fluence range are shown below:

Open Circuit Voltage

$$V_{oc} = V(o)\Big|_{\phi} + A \log\left(10^{-18}\frac{dN}{dx}\right) \qquad (1)$$

Maximum Power

$$P_m = P(o)\Big|_{\phi} - B \log\left(10^{-18}\frac{dN}{dx}\right) \qquad (2)$$

Short Circuit Current

$$I_{sc} = I(o)\Big|_{\phi} - C \log \left(10^{-18} \frac{dN}{dx}\right) \quad (3)$$

The slopes A, B, and C, determined from the measured data, are 16 mv/decade, 2.4 mv/decade, and 8.5 ma/decade respectively. The intercepts $V(o)|_{\phi}$, $P(o)|_{\phi}$ and $I(o)|_{\phi_4}$ represent values corresponding to the 1×10^{18} cm^{-4} gradient and have different magnitudes at each fluence level. In addition an empirical relationship for the 1 MeV electron damage coefficient (K_L) was determined from the I_{sc} bombardment behavior and is shown below.

$$K_L(o) = 5.3\times10^{-18} \left(\frac{dN}{dx}\right)^{1/2} (1 - 0.063 \log \phi) \quad (4)$$

THEORY

Description of 4-layer Model

The cell model shown in figure 1 is identical to the one used by Wolf (8) to calculate drift field cell collection efficiencies. The homojunction semiconductor device is divided into a diffused and a base region. Each region is further divided into two subregions resulting in four layers for the total structure. The subregion boundaries, Y and X, can be varied to alter the relative thickness of each subregion. The depletion region is not counted as a fifth layer since all photogenerated carriers in this region are assumed to be collected (i.e., 100% collection efficiency). The impurity concentrations shown in figure 2 are specified at the boundaries of the front and rear surface (0 and W), the subregions X, Y and the depletion region. This arrangement permits drift electric fields to be applied across the subregions. For this study only exponential impurity distributions are assumed which result in constant drift fields. Other cell properties used in calculations are shown in Table II. Individual subregion properties such as mobility (μ) and carrier lifetime (τ) can be specified independently. Additionally the surface recombination velocity for the rear (s_r) and front (s_f) surfaces are specified. The calculations are for a tungsten 2800 K spectrum except where noted.

The general approach to the solution of this model requires solving the continuity equation using the current transport equation and appropriate boundary conditions.

We have extended the work of Wolf (8) to permit evaluation of the open circuit voltage and maximum power, in addition to the short circuit current. Using the same boundary conditions at the subregion and front and rear surfaces, as cited in (8) an expression for the drift field diode saturation current (I_o) was derived, and is shown in Appendix A. Hence I_o reflects the four layer concept in that not only can the material properties of each sublayer be specified, but also that drift fields can be introduced via the exponential impurity distributions. Thus expressions for I_o and I_{sc} were programmed on a high speed digital computer and used to calculate the voltage from the expression

$$V_{oc} = \frac{kT}{q} \ln \left(\frac{I_{sc}}{I_o} + 1\right) \quad (5)$$

The maximum power was calculated using the well known relationship

$$P_{max} = CF \times V_{oc} \times I_{sc} \quad (6)$$

The curve factor (CF) was calculated using the equations and an iteration method proposed by Loferski (11). The overall computer program is arranged to permit performance analysis of a variety of cell designs and operating environments. The cell geometry, the depletion region width assuming an abrupt junction, material properties and drift field strength can be selected or calculated in addition to the choice of cell operating temperature and photon spectrum for either tungsten or sunlight. The cell spectral response can also be calculated. Reflection coefficients for either a bare or SiO coated cell can be selected to simulate the real cell, rather than assuming complete absorption.

Modeling of the Lithium Cell

The computational model used to represent the experimental cells was constructed in the following way. The lithium concentration from figure 2 is specified at the depletion region edge ($x \approx x_j$), at the subregion boundary, and at the rear contact $X = W$. Even though the real profile may be far more complex, the lithium concentration was approximated by an exponential increase from the depletion edge to the subregion boundary. From there to the ohmic rear contact, the lithium was assumed uniformly distributed and therefore field free. Thus, having specified the concentrations, the width of the subregion nearest the junction (i.e., field region width) was calculated using the experimental values for the lithium gradient and equation (B6) derived in Appendix B. (Conversely, given the concentrations and the field region width, the gradient could be calculated if so desired.) The field region widths calculated for the 1×10^{19} and 1×10^{18} cm^{-4} lithium gradients are about 3 and 11 μm respectively. These values are in reasonable agreement with the experimental data.

The selection of values for the various cell parameters also was based, where possible, on experimental data. The initial carrier lifetimes shown in Table I were based on the I_{sc} versus diffusion length data from Faith (12). The same lifetime was assumed for both subregions. The differing carrier mobilities shown in Table II reflect the difference in average lithium concentration of the two subregions. Other cell specifications used in the modeling are shown in Table II.

For the electron fluence range of zero to 3×10^{14} e/cm^2, the lithium cell performance was easily simulated assuming only diffusion length (lifetime) degradation and carrier removal effects. The changes in the initial diffusion length were calculated using the damage coefficients computed from equation (4). Carrier removal effects were simulated by reducing the initial lithium concentrations using a constant carrier removal rate (CRR) of 0.04 carriers/cm-electron.

At the 3×10^{15} e/cm^2 fluence the assumption of field removal, in addition to diffusion length and carrier removal effects, was necessary to simulate the measured data. Field removal was included by artificially reducing the electric field strength in the subregion nearest the junction. The field was decreased using a trial and error method until the voltages calculated for the 3×10^{15} e/cm^2 fluence were brought into agreement with the experimental data. It is obvious that this procedure "forced" the highest fluence voltages into agreement with the experimental trends. However the appropriateness of this approach was judged primarily by the magnitudes and trends that resulted for the short-circuit current and the maximum power.

RESULTS

Open-Circuit Voltage

The results of the calculations for the initial and bombarded V_{oc}, P_{max} and I_{sc} are shown in figure 3, for lithium gradients in the range of 10^{18} to 10^{19} cm^{-4}. The calculated data are based on lifetimes calculated from the empirical damage coefficients and for a constant CRR of about 0.04. Figure 3a shows the calculated voltage data as the open symbols compared to the empirical data, shown by the solid lines. The initial calculated voltages are representative of the range (error bars) of experimentally measured values corresponding to gradients of 10^{18}, 5×10^{18}, and 10^{19} cm^{-4}. In general it was found that the initial voltages depend strongly on the lithium concentration at the depletion region edge, and to a lesser degree on the initial carrier lifetime. The agreement between the calculated and experimental trends at the three fluence levels is excellent. The fall off of voltage being about 16 mV/decade; in agreement with experiment.

Decreases in the lithium gradient are predicted above 3×10^{14} e/cm and are shown in the figure. These changes are due to carrier removal effects and are most severe for the lowest gradient due to an overall lower lithium concentration in that cell. It was found that lifetime degradation and carrier removal alone would result in a slope at the 3×10^{15} e/cm^2 level that was much steeper than that indicated by the experimental data. Agreement was achieved, however, by artificially reducing the drift field to simulate radiation induced field removal. Although there is no experimental evidence suggesting that field removal does indeed occur, Dresselhaus (13) suggests that mobile negatively charged radiation induced defects (1, 14) can drift within the field region. If this were the case a counter field would arise weakening the lithium drift field.

Maximum Power

Figure 3b shows the initial and bombarded trends predicted for the maximum power. The calculated curve factors of about 0.80 were reduced by 8% to more closely agree with experimental data. These data correspond to the same conditions as discussed for the voltage. The solid lines represent the empirical data, while the broken lines and open symbols show the calculated trends. The experimental data were converted to a power density by assuming an active area of 1.8 cm^2. The disagreement between the experimental and the calculated power densities is about 5 to 10%. The predicted slopes are slightly steeper but yet in reasonable agreement with the empirical trends. As shown in Table III, the calculated range is 3.33 to 2.46 mW/decade compared to the average experimental value of 2.40 mW/decade.

Short-Circuit Current

The predicted short-circuit current densities (broken lines and open symbols) are shown in figure 3c, and are again compared with the empirical trends (solid lines). The experimental current densities were calculated assuming an active area of 1.8 cm^2. As can be seen the predicted dependence of current on lithium gradient is in reasonable agreement with experiment. These slopes are compared in Table III. The calculated values range from 8.91 to 8.37 ma/decade compared to the experimental average of 8.5 ma/decade. It is perplexing, however, that the magnitudes of the calculated current density at the 3×10^{13} and 3×10^{15} e/cm^2 fluences are in disagreement by about 10% with the measured data. The current is underestimated at 3×10^{13} e/cm^2, but overestimated at the 3×10^{15} fluence level.

Since the current is more sensitive than the V_{oc} or P_m to intensity, spectrum, and diffusion length, failure to closely simulate the experimental conditions would have a more pronounced effect on the current. Furthermore, the radiation damage trends are found to be sensitive to the character of the light source. Figure 4 shows the results of the I_{sc} calculation where the AMO sunlight spectrum was substituted for the tungsten 2800° K spectrum used previously. Not only is the slope significantly shallower (4.8 ma/decade) than for the tungsten case, but the AMO current densities are also about 16% higher. These results are not unexpected since it is well known that a radiation damaged cell will appear more severely degraded when evaluated with a red-rich light source compared to a similar evaluation with a blue peaked source. This shows that in addition to the intensity, the spectrum of the light source plays a significant role in determining a cell's radiation performance trends as a function of lithium gradient.

CONCLUSION

The four layer drift field model was used to predict the pre- and post-irradiation performance of the lithium solar cell. Using this model and published experimental data for the C-13 group of lithium cells the V_{oc}, I_{sc}, and P_m were calculated and compared with the measured performance. The empirically determined dependence of these parameters on electron fluence and lithium gradient has been verified using this model and by assuming diffusion length degradation, and carrier removal. For fluences above 3×10^{14} e/cm^2 the added assumption of field removal was made. Calculations using an AMO light source spectrum predict that the rate of change of the performance parameters with lithium gradient is less than when measured under tungsten illumination.

It is concluded that this model can be applied generally to explain the performance of all lithium cells providing sufficient information is available concerning the lithium profile and the minority carrier lifetime, as well as the character of the light source.

APPENDIX A - SATURATION CURRENT

Using the model shown in figure 1, the n-base component of the diode saturation current density is derived from the continuity and the current transport equations. The treatment is identical for the p-base component. Hence, for the one dimensional case, the general differential equation can be written in the steady state

$$\frac{d^2n}{dx^2} + \frac{qE}{kT}n - \frac{n}{L_n} = 0 \qquad (A1)$$

where E is the constant drift field and L_n the n-base bulk diffusion length. Equation (A1) has the general solution

$$n(x) = D_1 e^{r_1 x} + D_2 e^{r_2 x} \qquad (A2)$$

where

$$r_1 = -\frac{qE}{2kT} + \left[\left(\frac{qE}{kT}\right)^2 + \left(\frac{1}{L_n}\right)^2\right]^{1/2}$$

r_2 is similar except that the 2nd term has a negative sign instead of positive. A similar solution with different coefficients is written for the second subregion. Equation (A2) is the general expression for the minority carrier density in the n-base. The drift field solution is obtained by solving for the coefficients subject to the following boundary conditions:

1. at $x = x_j$

$$n(x_j) = \frac{n_i^2}{N_D} (\exp \beta V - 1)$$

where $\beta = q/kT$, n_i the intrinsic concentration, and N_D the lithium concentration at the junction edge.

2. at $x = X$

$$n_1(X) = n_2(X)$$

$$D_{n_1} \frac{dn_1(X)}{dx} + \mu_{n_1} E_1 n_1(X) = D_{n_2} \frac{dn_2(X)}{dx} + \mu_{n_2} E_2 n_2(X) \qquad (A3)$$

where the subscripts 1 and 2 refer to the subregion nearest the junction and nearest the contact respectively.

3. at $x = W$

$$\frac{dn_2(W)}{dx} = - S_2 n_2(W)$$

where

$$S_2 = \frac{qE_2}{kT} + \frac{s_r}{D_{n_2}}$$

and s_r is the surface recombination velocity.

After an algebraic manipulation, the following expression is obtained for the diode saturation current

$$I_{o_n} = -qD_{n_1} \frac{n_i^2}{N_D} \left[\frac{\left(CB_1 + A_1 \exp^{(B_1 - A_1)x_j} \right) + 2F_{n_1} \left(C + \exp^{(B_1 - A_1)x_j} \right)}{C + \exp^{(B_1 - A_1)x_j}} \right]$$

where

$$A_m = \frac{qE_{nm}}{2kT} - \left[\left(\frac{qE_{nm}}{2kT} \right)^2 + \left(\frac{1}{L_{nm}} \right)^2 \right]^{1/2} \cong F_{nm} - G_{nm} \qquad (A4)$$

$$B_m = F_{nm} + G_{nm}$$

where $m = 1$ is the subregion nearest the junction, $m = 2$, nearest the contact; and

$$C = \frac{\left(\frac{S_2 - A_2}{S_2 - B_2} \right) \exp^{2G_{n_2}(W-X)} \left[B_1 - \gamma A_2 \right] + \left[B_1 - \gamma B_2 \right] \exp^{2G_{n_1}X}}{\left(- \frac{S_2 - A_2}{S_2 - B_2} \right) \exp^{2G_{n_2}(W-X)} \left[\gamma A_2 - A_1 \right] + \left[\gamma B_2 - A_1 \right]}$$

$$\gamma = \frac{D_{n_2}}{D_{n_1}}$$

A similar equation can be derived for the diffused layer. Therefore the total diode saturation current used to calculate the open-circuit voltage can be written

$$I_o = I_{o_n} + I_{o_p} \qquad (A5)$$

APPENDIX B - FIELD REGION WIDTH

The field region width was calculated by assuming lithium concentration (N_2) at the depletion edge (x_j) that increases exponentially to the subregion boundary X. The width of this subregion is therefore ($X - x_j$). The concentration (N_H) is assumed constant from the subregion boundary ($x = X$) to the rear contact ($x = W$). The lithium concentration within the subregion ($X - x_j$) can be expressed

$$N_1(x) = N_o \exp ax \qquad (B1)$$

where a is the grade constant. (B1) is subject to the boundary condition:

$$\text{at } x = x_j\text{: } N(x_j) = N_o \exp ax_j = N_L; \qquad (B2)$$

$$\text{at } x = X\text{: } N(X) = N_o \exp aX = N_H$$

The lithium gradient is given by

$$\frac{dN}{dx} = aN_o \exp ax \qquad (B3)$$

evaluating (B3) at the depletion region edge $x = x_j$

$$\left. \frac{dN}{dx} \right|_{x = x_j} = a N_L \qquad (B4)$$

From (B2), the grade constant can be determined

$$a = \frac{\ln \frac{N_H}{N_L}}{X - x_j} \qquad (B5)$$

Substituting (B5) into (B4) and solving for $X - x_j$

$$X - x_j = N_L \frac{\ln \frac{N_H}{N_L}}{\left. \frac{dN}{dx} \right|_{x = x_j}} \qquad (B6)$$

REFERENCES

1. Joseph J. Wysocki, "Role of Lithium in Damage and Recovery of Irradiated Silicon Solar Cells." IEEE Transactions on Nuclear Science, Vol. NS-14, No. 6, December 1967.

2. P. H. Fang, Y. M. Liu, "Interaction of Lithium with Impurities and Defects in Silicon." Vol. 9, No. 10, Applied Physics Letters, November 15, 1966.

3. J. J. Wysocki, P. Rappaport, E. Davison, R. Hand, J. J. Loferski, "Lithium-Doped, Radiation-Resistant Silicon Solar Cells, Vol. 9, No. 1, Applied Physics Letters, July 1, 1966.

4. T. J. Faith, "Voltage and Power Relationships in Lithium-Containing Solar Cells," Photovoltaic Specialists Conference, May 2-4, 1972.

5. T. J. Faith, "Damage and Recovery Characteristics of Lithium-Containing Solar Cells," IEEE Transactions on Nuclear Science, December 1971, p. 371.

6. P. A. Iles, "Development and Fabrication of Lithium-Doped Solar Cells," Proc. 4th Annual Conference on Effects of Lithium Doping on Silicon Solar Cells, JPL, April 29, 1971, p. 13.

7. T. J. Faith, A. G. Brucker, A. G. Holmes-Siedel, and R. S. Neadle, IEEE Transactions on Nuclear Science, NS-15, 61 (Dec. 1968).

8. M. Wolf, "Drift Fields in Photovoltaic Solar Energy Converter Cells," Proc. IEEE, Vol. 51, May 1963, 674-693.

9. W. R. Runyan, and E. G. Alexander, "An Experimental Study of Drift-Field Silicon Solar Cells," IEEE Transactions on Electron Devices, Vol. Ed-14, No. 1, January 1967.

10. Roger Van Overstraeten, and Walter Nuyts, "Theoretical Investigation of the Efficiency of Drift-Field Solar Cells," IEEE Transactions on Electron Devices, Vol. Ed-16, No. 7, July 1969.

11. J. J. Loferski, "Theoretical Considerations Governing the Choice of the Optimum Semiconductor for Photovoltaic Solar Energy Conversion," Journal of Applied Physics, Vol. 27, No. 7, July 1956.

12. T. J. Faith, Jr., "Density and Fluence Dependence of Lithium Cell Damage and Recovery Characteristics," JPL, April 29, 1971, p. 13.

13. M. S. Dresselhaus, "Radiation Damage Annealing Kinetics," ibid, p. 101-113.

14. G. O. Watkins, J. Phys. Soc. Japan 18, 22 (1963).

TABLE I

PUBLISHED EXPERIMENTAL DATA FOR C-13 GROUP OF LITHIUM CELLS - REFS. 5 AND 12

		High Gradient (375°C-180 min)	Low Gradient (325°C-480 min)
Lithium Concentration(1) atoms/cm^3	$x=x_j$	8×10^{14}	3×10^{14}
	x=X	5×10^{16}	1×10^{16}
	x=W	5×10^{16}	1×10^{16}
Gradient, atoms/cm^4		1×10^{19}	1×10^{18}
Initial Lifetime (N-base)(2), μsec		10	27
Subregion Width(3), μm		~3	10-20

TABLE II

ASSUMED OR CALCULATED DATA USED IN LITHIUM CELL MODELLING

		High Gradient	Medium Gradient	Low Gradient
Field Region (X-x_j)		3.0	6.6	11.1
Junction Depth (x_j)		← 0.25 →		
Cell Thickness (μm)		← 375 →		
Mobility, cm^2/volt-sec	(X-x_j) Region	← 500 →		
	(W-X) Region	300	300	400
Diffusion Region Profile		erfc (1/3 Dead Layer)		
Surface Recombination Velocity, cm/sec	Front	← 10^5 →		
	Rear	← 10^8 →		
AR Coating		← SiO →		
Lithium Gradient, atoms/cm^4		1.1×10^{19}	5×10^{18}	9.5×10^{17}

TABLE III

CALCULATED AND EXPERIMENTAL RADIATION DAMAGE DATA FOR I_{SCC} AND P_{MAX} FOR HIGH AND LOW GRADIENT LITHIUM DRIFTED SOLAR CELLS

Current (I_{SCC})		
Electron Fluence, e/cm^2	$\frac{\Delta I\ (A=1.8\ cm^2)}{\text{Decade}}$	Experimental Slope*
3×10^{13}	8.46	8.4
3×10^{14}	8.91	8.4
3×10^{15}	8.37	8.9
Average	8.4	8.5
Maximum Power		
Electron Fluence, e/cm^2	$\frac{\Delta P\ (A=1.8\ cm^2)}{\text{Decade}}$	Experimental Slope*
3×10^{13}	3.33	2.39
3×10^{14}	3.24	2.40
3×10^{15}	2.46	2.42
Average	3.01	2.40

* Refs. 4 and 5

CROSS SECTION OF FOUR LAYER MODEL
OF LITHIUM SOLAR CELL

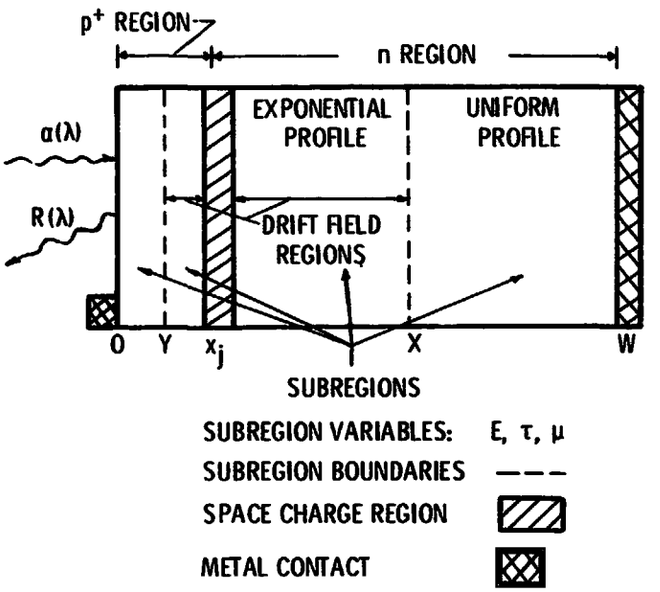

Fig. 1

LITHIUM PROFILE AND FIELD REGION WIDTHS

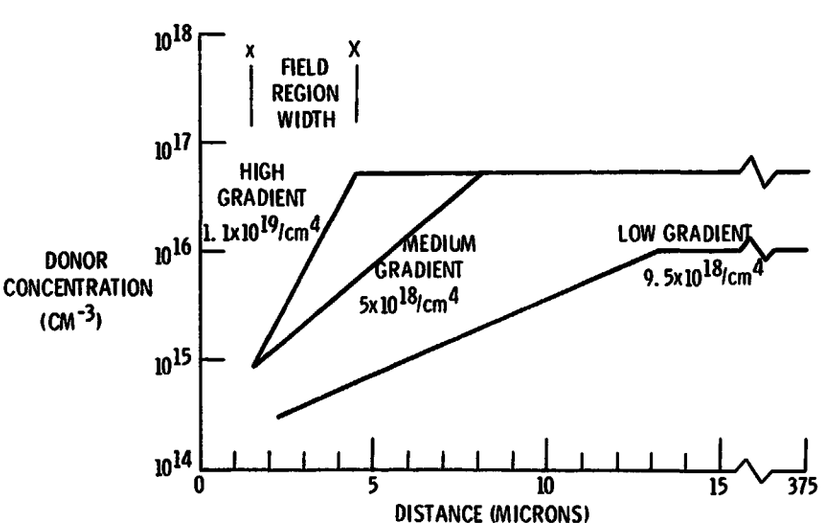

Fig. 2

OPEN CIRCUIT VOLTAGE IMMEDIATELY AFTER IRRADIATION
VERSUS LITHIUM GRADIENT FOR TUNGSTEN 2800K SPECTRUM

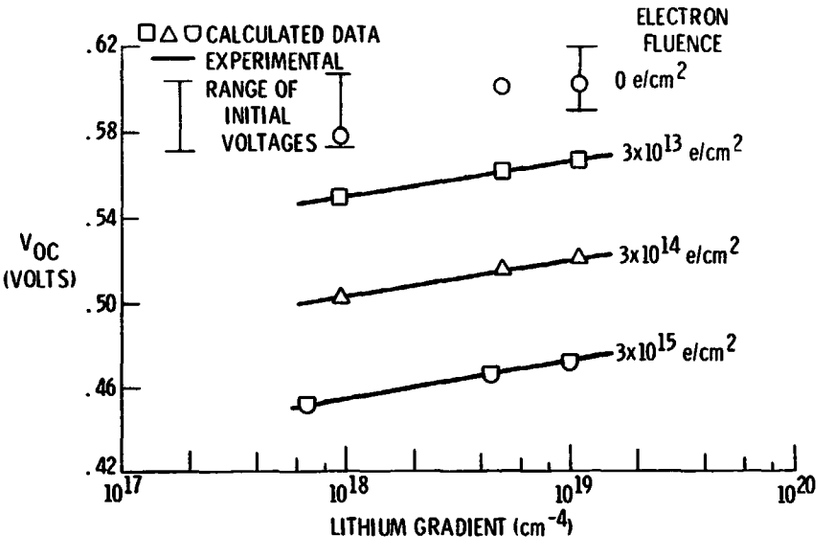

Fig. 3a

E-7(25

MAXIMUM POWER IMMEDIATELY AFTER IRRADIATION AGAINST
LITHIUM GRADIENT FOR TUNGSTEN 2800K SPECTRUM

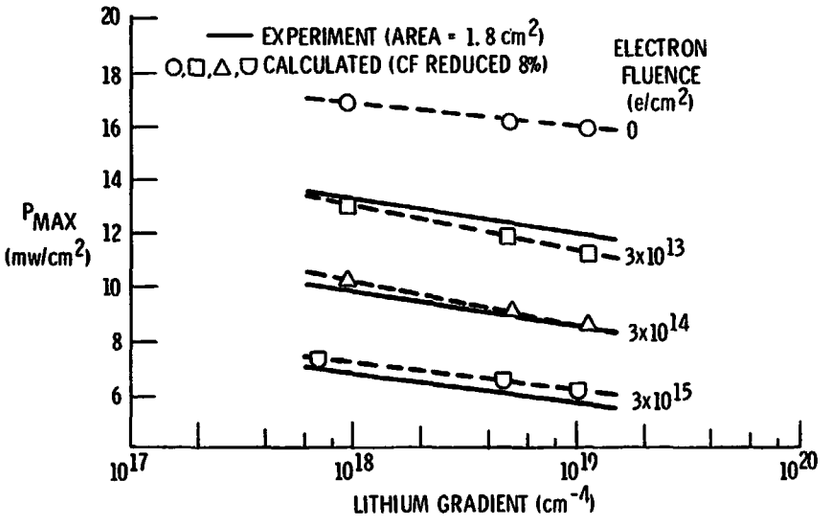

Fig. 3b

SHORT CIRCUIT CURRENT IMMEDIATELY AFTER
IRRADIATION AGAINST LITHIUM GRADIENT
FOR TUNGSTEN 2800K SPECTRUM

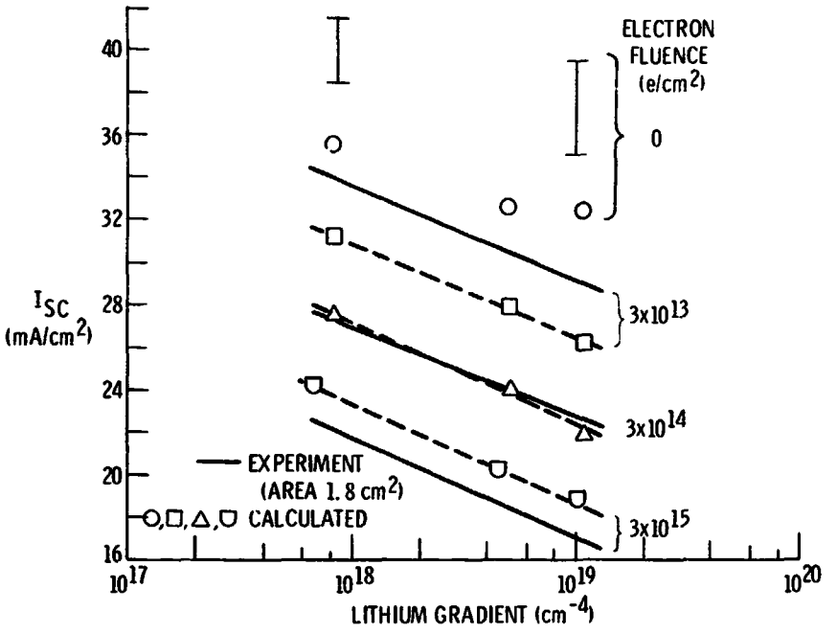

Fig. 3c

E-7025

CALCULATED RADIATION BEHAVIOR OF SHORT CIRCUIT
CURRENT DENSITY FOR AIR MASS ZERO SPECTRUM

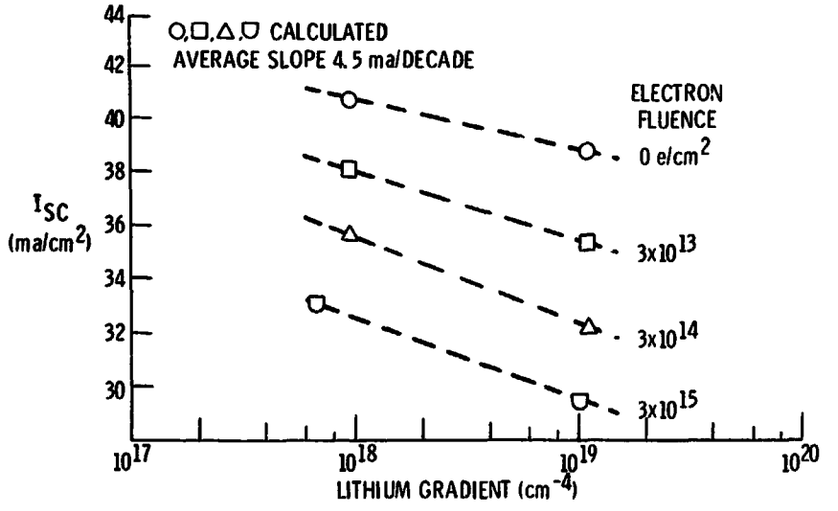

Fig. 4

NASA-Lewis